18TH WORLD CONFERENCE ON EARTHQUAKE ENGINEERING
WCEE2024
MILAN

MILAN, ITALY
30TH JUNE - 5TH JULY 2024

www.wcee2024.it

REGIONAL SEISMIC RISK ASSESSMENT INCLUDING LIQUEFACTION AND SEA LEVEL RISE

E. Mongold[1], J. Sobers[2] & J.W. Baker[2]

[1] Stanford University, Stanford, CA, USA, emongold@stanford.edu

[2] Stanford University, Stanford, CA, USA

Abstract: *At a regional scale, damage and loss from earthquakes can come largely from ground failures driven by mechanisms such as liquefaction. Future rising sea levels are expected to raise the groundwater table in coastal areas, exacerbating liquefaction in the event of an earthquake. Past regional liquefaction studies have been limited by not considering multiple earthquake events, and changes in groundwater. This study bridges those gaps through a regional hazard analysis of probabilistic future earthquakes that can be combined with loss and recovery simulation. We provide a framework to simulate current and future regional soil and groundwater properties under sea level rise.*

1. Introduction

Liquefaction is a phenomenon causing ground failure during earthquakes. Coarse grains of saturated soil become suspended in the pore water during ground shaking, and the entire soil matrix acts as a liquid. This can cause several surface impacts including sand boils, lateral spreading, and uneven settlement, with physical impacts such as broken pipes, cracked pavement, and foundation settlement (National Academies of Sciences, Engineering, and Medicine, 2021). Liquefaction has been observed after many earthquakes (e.g. van Ballegooy et al. 2014). Liquefaction can cause extensive damage yet is not always considered in earthquake risk analyses, and research within geotechnical engineering mostly investigates triggering (e.g. Holzer et al. 2011, Todorovic and Silva 2022, Zhu et al. 2017). The liquefaction potential index (LPI) is a metric developed by Iwasaki et al. (1978), that aggregates liquefaction potential over a soil column. Numerous functions for LPI have been fit to empirical data (e.g. Moss et al. 2006, Boulanger and Idriss 2014), and these LPI-based methods have been related to severity or manifestation (e.g. Holzer et al. 2002, Kim et al. 2021). Some work has been done to expand the methods to further assess the severity of liquefaction, probability of liquefaction, impacts on structures, and regional analysis (e.g. Li et al. 2006, Wu et al. 2020); however, few studies perform a comprehensive probabilistic liquefaction hazard analysis (National Academies of Sciences, Engineering, and Medicine, 2021). Probabilistic liquefaction hazard analysis combines the probability of liquefaction occurrence with the likelihood of triggering earthquakes, resulting in annual rates of liquefaction (Goda et al. 2011).

A less common piece of the liquefaction hazard framework translates ground failure into damage to the built environment. Liquefaction is a concern for structures, buried pipes, roadways, and other infrastructure (National Academies of Sciences, Engineering, and Medicine, 2021). Risk analysis uses models that predict the probability of damage, categorized as a damage state, given a hazard intensity, known as fragility functions. Though damage states and fragility functions are common in earthquake engineering, liquefaction

fragility functions are uncommon and often rely on input intensity measures such as ground deformation (e.g. Bird et al., 2006), which is not predicted in an LPI-based method. They also require information about the foundation and bearing pressure of buildings (Sahir and Pak, 2010), which would require additional assumptions about the building stock. Other models use peak ground acceleration (PGA) as the input, which ignores the soil type and groundwater level (Koutsourelakis et al., 2002), or are conditioned on groundwater depth and earthquake magnitude (Holzer et al., 2011). Other simplified models such as HAZUS may be used, especially for regional-scale analysis, for an aggregate sense of impacts on built infrastructure (FEMA, 2020). Though many methods exist to quantify liquefaction hazard, they do not seamlessly fit together for a complete risk analysis.

For soils to liquefy, they must be saturated and, thus, must be lower than the groundwater table. Liquefaction probability varies seasonally because of the changing groundwater table (Pokhrel et al., 2022) and reaches higher thresholds as groundwater becomes shallower (Chung and Rogers, 2013). As sea level rise (SLR) is expected to cause shallow coastal groundwater to shoal, more soil will be susceptible to liquefaction in coastal areas. This change will affect the soil closest to the surface, which will become newly saturated and is most likely to cause surface manifestation. Thus, small increases in liquefiable soil close to the surface may have a large impact on the liquefaction potential of a site and, on a regional scale, increase the extent of a community that may experience liquefaction. Some regional studies have examined how the rising sea level may alter the liquefaction risk around the San Francisco Bay area (Wang et al., 2021; Wang and Chen, 2018; Grant et al., 2021). They all found that the hazard extent will increase; however, they use many simplifying assumptions and are conditioned on earthquake events, leaving gaps in our understanding of the full change in hazard and risk.

This paper describes a regional probabilistic liquefaction model that includes changing groundwater levels under sea level rise scenarios. Our model integrates changes in groundwater data and is applied to a case study in Alameda, California, USA. Alameda is a city located on a liquefaction-susceptible island in the San Francisco Bay. The preliminary results show that sea level rise is expected to increase the liquefaction hazard in the region, with both higher severity and wider areas that may be impacted. This approach will enable us to assess risk due to losses from ground shaking and liquefaction and assess how households may be impacted under future conditions.

2. Model setup

This paper focuses on the addition of sea level rise (SLR) to probabilistic regional liquefaction hazard and risk analysis. We use the framework developed by Mongold and Baker (forthcoming) with minor adjustments. The input data requirements include soil properties, groundwater, and ground shaking across the study area. Geospatial simulation is used to generate data across the region between known, measured data points. Liquefaction potential index (LPI) is the metric we use to proxy liquefaction severity. LPI depends on all the data mentioned above, calculated as

$$LPI = \int_{wd}^{20m} (1 - FS) \cdot w(z)dz \tag{1}$$

where wd is the depth from the ground surface to the groundwater table, w(z) is a weighting factor, linearly decreasing with depth, and FS is the factor of safety, calculated as

$$FS = \frac{CRR}{CSR} \tag{2}$$

where CRR is the cyclic resistance ratio and CSR is the cyclic stress ratio, representing the strength of soil and the load induced by the earthquake ground shaking. Both of these parameters are determined by empirical LPI equations (Moss et al. 2006, Boulanger and Idriss 2014).

Figure 1 shows the overall workflow with consideration of sea level rise. One set of input parameters is used to generate soil and ground shaking simulations. Thus, the only change between each SLR scenario is the groundwater level and its effect on the soil properties, such as effective vertical stress. Each of these combinations of inputs are run through the main liquefaction calculations. An output is generated for each SLR scenario that includes expected LPI maps and the rate of liquefaction.

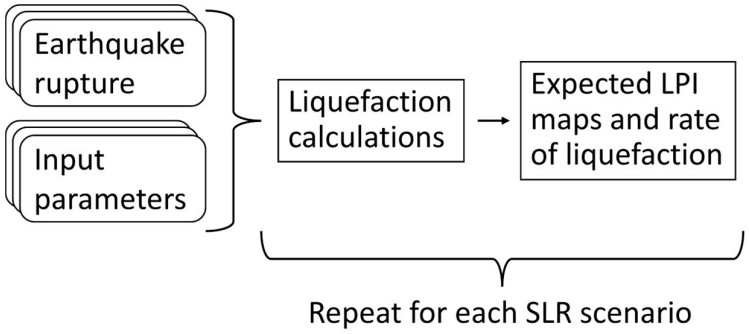

Figure 1. Schematic of simulation flow with multiple sea level rise (SLR) scenarios.

2.1. Groundwater table

The groundwater table in coastal areas is expected to change under sea level rise (Befus 2020a), and has been modelled by multiple agencies (e.g. Befus 2020b, May et al. 2022). These models are used as input to the groundwater table across a region of interest. The first step is to choose a data source and the second is to join the groundwater data with the points across the case study area.

We utilize water table projections from the United States Geological Survey (USGS) in this work (Befus 2020b). There are other options for this data, notably from a San Francisco Estuary Institute (SFEI) report (May et al. 2022). Both data sources include many SLR scenarios, with USGS having 12 and SFEI having 10. While SFEI uses a linear model focusing on near-shore areas, USGS has a full MODFLOW model to run homogenous, steady-state equations (Hughes et al. 2017). The USGS data also incorporates multiple values of marine boundary conditions, at mean higher-high water (MHHW) level and local mean sea level (LMSL) and three values of hydraulic conductivity, 0.1m/day, 1.0m/day, and 10m/day. SFEI uses bay tidal datums to estimate slope towards the bay and approximates the potential drainage of groundwater due to tributaries and lagoons. The USGS models unconfined water tables under natural conditions, and the SFEI focuses on the highest annual level of groundwater. Finally, USGS is fully simulated, while SFEI is based on groundwater data and past modelling. Both data sources are useful in their own contexts, but for the case of probabilistic analysis, we utilize the USGS data due to its additional variation of marine boundary condition and hydraulic conductivity, and that it represents a more moderate value, as opposed to focusing on the highest water level.

Once the data source is chosen, some pre-processing is necessary to use the data in the analysis. Points across the island are used to perform the regional analysis. Water depth is interpolated from nearby data to the points across the study area. However, applying groundwater data to these points can cause multiple challenges. The first challenge is that some points in the study area are considered to be submerged underwater in the groundwater data (black ‘X’ in Figure 2). This discrepancy occurs when points are very close to the shore or after sea level rise has caused them to become underwater. In these submerged cases, the point is assumed to have groundwater at the ground surface for liquefaction calculations and is flagged as being submerged. The second challenge that can occur is that points are missing values, where there is no data from the groundwater model (red ‘X’ in Figure 2). This may occur far from the shore or at edges of geographic boundaries such as county lines. These points can be extrapolated from nearby data. A threshold value of -135 is used as a cutoff in case the point is near one submerged datapoint, which weighs as -500. If the point is not submerged, then the value is interpolated from only existing data on land (not submerged), the same method as the interpolated points. The submerged points have a water depth of 0m and are marked as submerged so that they can be considered in future analysis. This process results in values of depth to groundwater for each point of interest within the case study area.

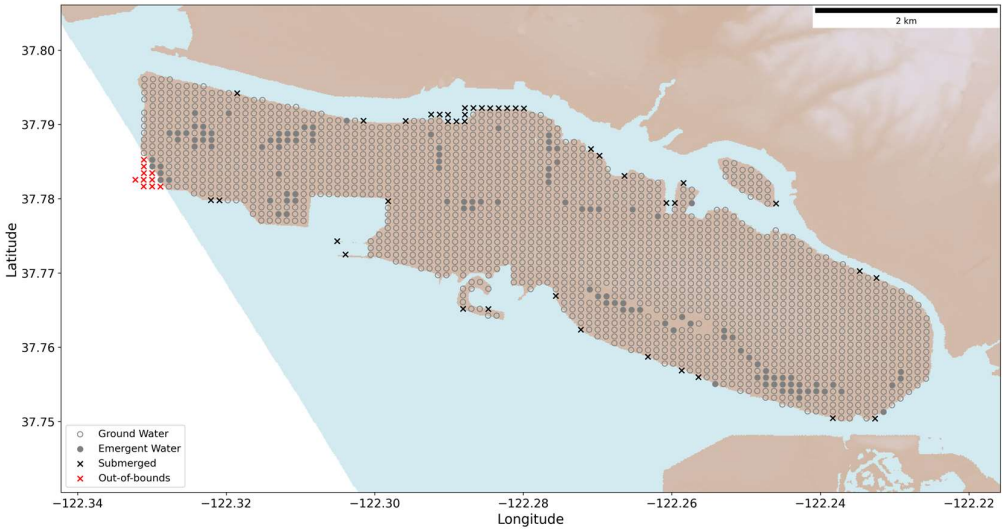

Figure 2. Plot of points across Alameda over the groundwater data, where blue is coastal water and brown is land. Round points indicate valid groundwater levels, and 'X' indicate challenging points, either submerged or out-of-bounds. Map is for MHHW with 1.0m/day hydraulic conductivity and 0m of SLR.

This groundwater pre-processing produces depths to groundwater for points across the case study area for each marine boundary condition and hydraulic conductivity value. Figure 3 shows the baseline case (0m of SLR) with LMSL and 1.0m/day hydraulic conductivity. The edges and western side of the case study area exhibit the shallowest groundwater, with a deeper water table in the inland eastern parts of the island.

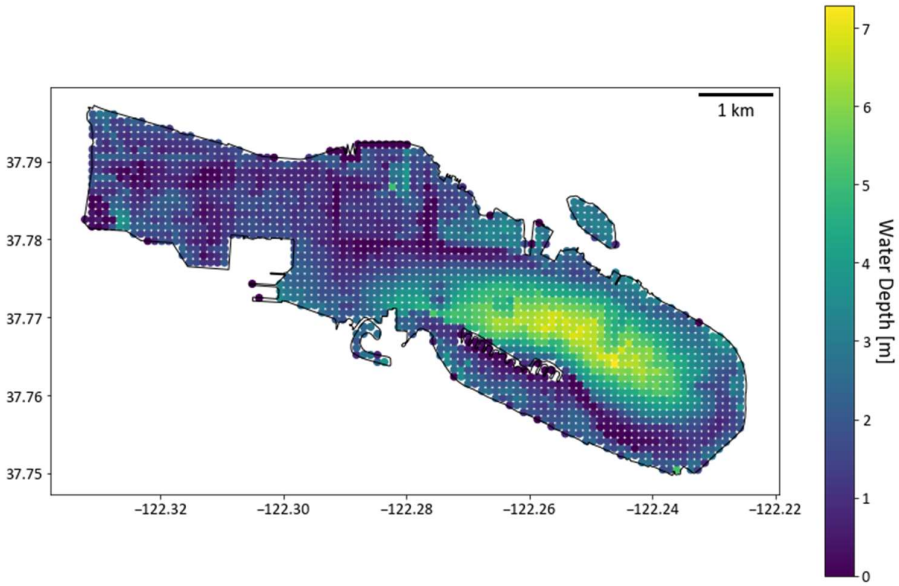

Figure 3. Depth to groundwater for sea level rise scenario of 0m, lower mean sea level tide, and 1m/day hydraulic conductivity.

The rise in groundwater due to SLR is shown in Figures 4 and 5, for 1m and 2m of SLR, respectively. Both are shown from 0m of SLR as a baseline (Figure 3). These changes are for LMSL and 1m/day hydraulic conductivity. Both of these SLR cases show that most locations exhibit a rise in the groundwater table, with points closer to the shoreline having a larger magnitude of rise. Points shown in white in Figures 4 and 5 do not exhibit a change in depth to groundwater under the sea level rise scenario. For this combination of marine boundary condition and hydraulic conductivity, few locations remain the same. A lower hydraulic conductivity value (0.1 m/day) results in more white space, or fewer locations with a rise in groundwater. A higher hydraulic

conductivity (10 m/day) results in more widespread rise in the groundwater across the case study area. Better-constrained hydraulic conductivity values would decrease uncertainty in the groundwater input maps.

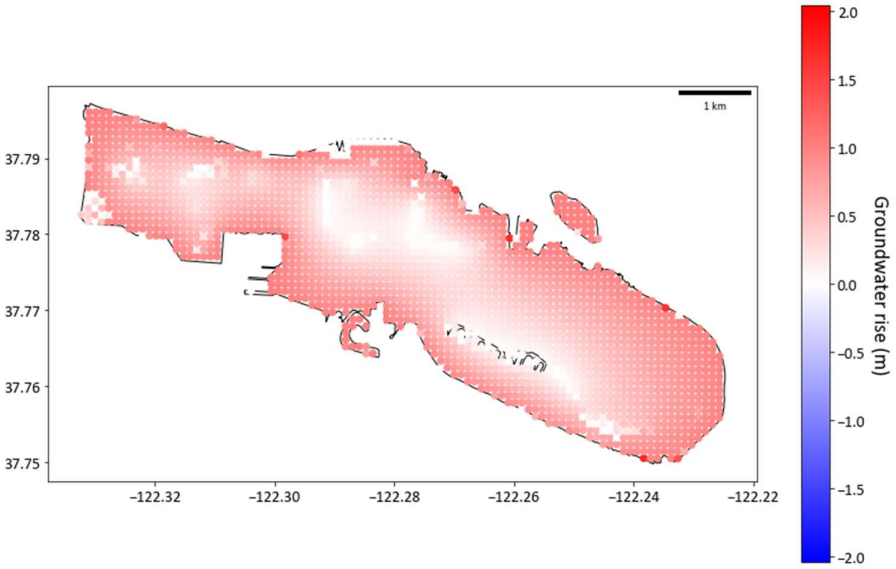

Figure 4. Rise in groundwater for sea level rise scenario of 1m, lower mean sea level tide, and 1m/day hydraulic conductivity.

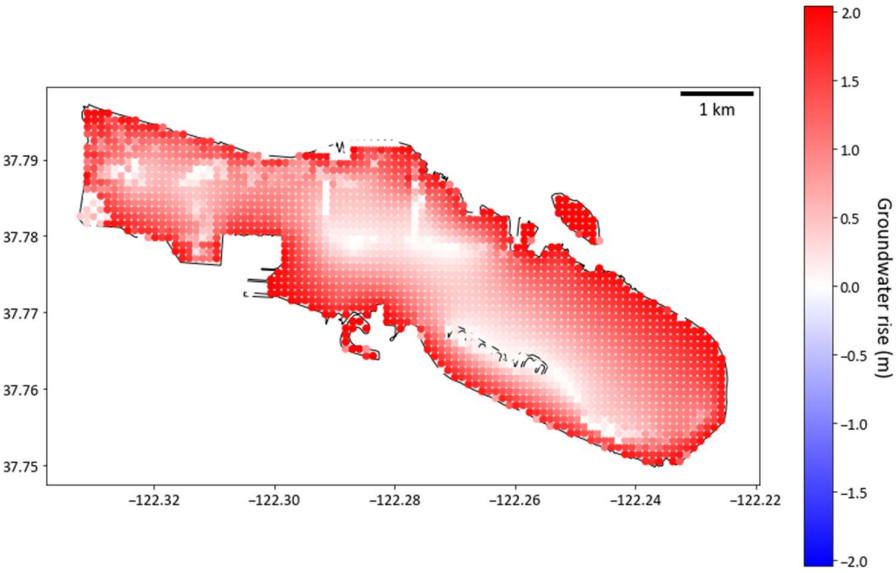

Figure 5. Rise in groundwater for sea level rise scenario of 2m, lower mean sea level tide, and 1m/day hydraulic conductivity.

2.2. Parameter uncertainty

For the probabilistic analysis, uncertain parameters are varied to include epistemic uncertainty in the modeling. These parameters fit into four main categories: ground motions, groundwater, soil, and liquefaction. Uncertainty in ground motions is included by using three ground motion models, each with equal probability of being chosen. Uncertainty in groundwater is included with equally weighted selection between three hydraulic conductivity values and two marine boundary conditions. Uncertainty in soil values is included in the geostatistical modeling parameters that define correlation in various directions and inherent randomness, represented by a variogram. The variogram includes three key parameters of major range, minor range, and

nugget. Finally, uncertainty in the liquefaction calculation comes by choosing between two empirical equations, and by varying the fines content constant in the Boulanger and Idriss (2014) equation.

Table 1. Input parameters treated as uncertain in the analysis. U[a, b] denotes a uniform distribution between a and b. Entries in lists of models or parameter values are treated as equally likely.

Category	Variable	Parameter range/ modelling source
Ground motions	Ground motion model	Abrahamson et al. (2014), Boore et al. (2014) or Chiou and Youngs (2014)
Groundwater	Hydraulic conductivity [m/day]	0.1, 1.0, 10
	Marine boundary condition	LMSL, MHHW
Soil	Variogram major range [km]	U[1.5,3.0]
	Variogram minor range [m]	U[8,15]
	Variogram nugget	U[0.00016,0.2]
Liquefaction	Empirical equation	Moss et al. (2006) or Boulanger and Idriss (2014)
	Fines content constant	U[-0.3,0.3]

3. Preliminary results

These preliminary results show the expected liquefaction potential index across the island of Alameda in current conditions, as well as under 1m and 2m of SLR. This expected LPI accounts for 2430 possible earthquake ruptures of magnitude 5.0 and above. Figure 6 shows the expected LPI given an earthquake across the study area. This weighting of being conditional on an earthquake event allows for easier interpretation of the values than pure expected LPI values. For a single scenario, LPI of 5 or above is generally associated with liquefaction (Iwasaki et al. 1978). The locations with above 5 expected LPI are likely to see liquefaction in many of the earthquake events considered, potentially with higher values for the stronger earthquake events. Figure 6 shows that liquefaction hazard is not uniform across the island but is concentrated on the northwest and southeast parts of the island.

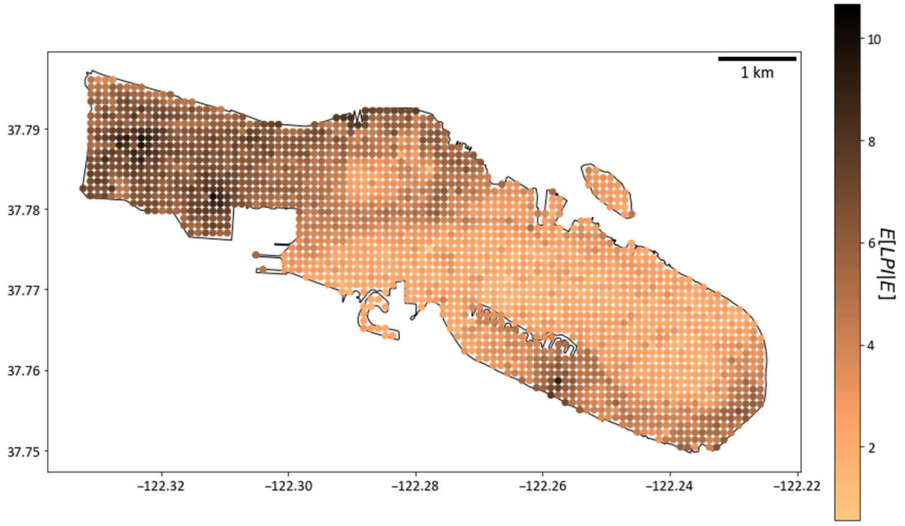

Figure 6. Expected LPI given an earthquake across the study area of Alameda for the baseline (0m of SLR).

With a change in groundwater level due to sea level rise, new expected LPI values are calculated by repeating the procedure for the SLR cases. The change in expected LPI value for 1m of SLR is shown in Figure 7, with darker red color indicating a larger increase in LPI. This increase is on the order of 1, and while a few points have a decrease in expected LPI, this value is of a small magnitude, less than 0.5, and would not change the interpretation from a change of 0.

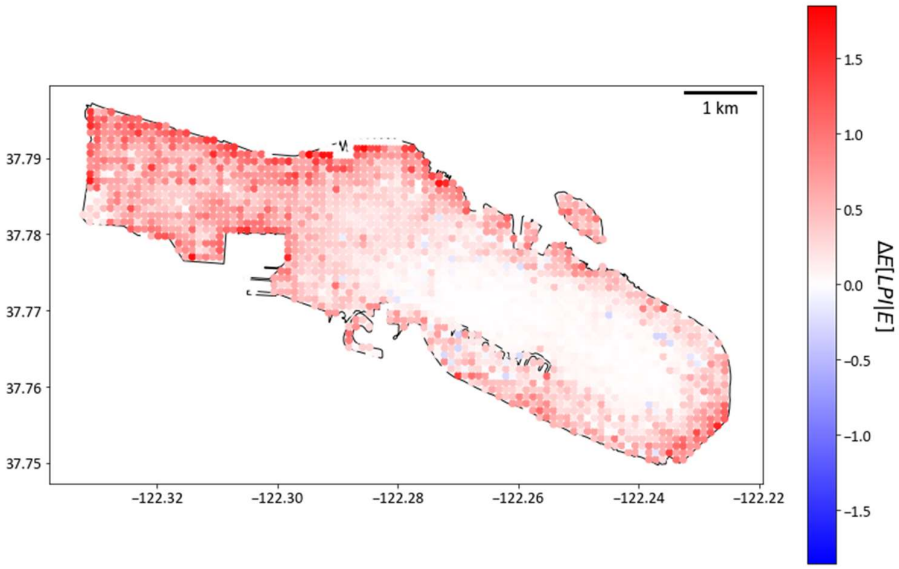

Figure 7. Change between 0-1m SLR in expected LPI, given an earthquake.

A similar trend is visible in Figure 8, showing the change from 0 to 2m of SLR. Figure 8 shows even fewer points with a decrease in expected LPI, and a larger magnitude for the points with an increase, going up to a change of 3. Most of the points with increase are along the areas with already large expected LPI values, and along the coastal edges of the island.

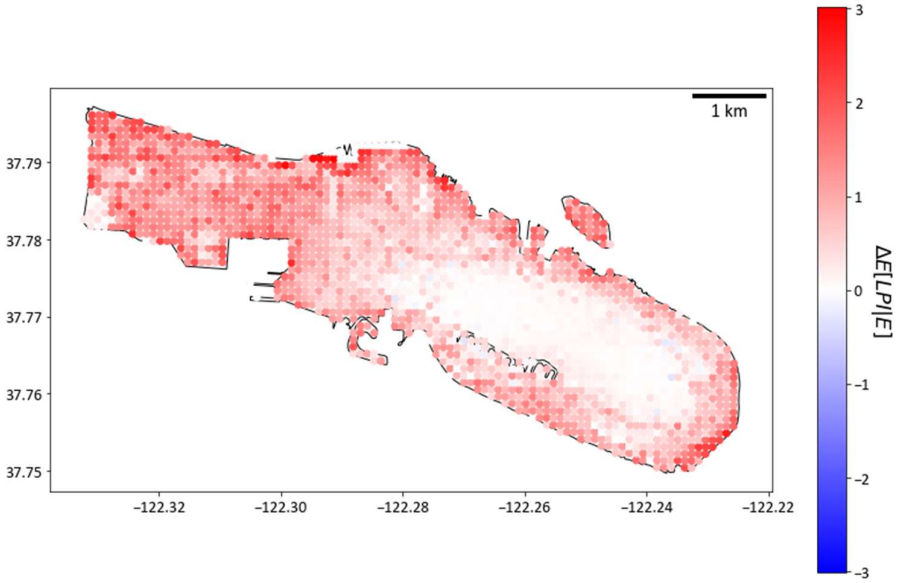

Figure 8. Change between 0-2m SLR in expected LPI, given an earthquake.

4. Conclusions

In this paper we have demonstrated a method to incorporate sea level rise into probabilistic liquefaction hazard analysis. This method includes new data sources of groundwater table predictions given various levels of sea

level rise, and accounts for uncertainty in boundary marine conditions and hydraulic conductivity. This approach is demonstrated for a case study in Alameda, CA, USA, where there is significant earthquake and liquefaction hazard. The treatment of unknown or underwater points permits assessment of changing conditions under sea level rise and correction for the bounds of data collection. The preliminary results show that liquefaction hazard is expected to increase in coastal locations, including in areas that already have high liquefaction hazard. This model can be incorporated into a seismic risk assessment to determine changes in the contribution of liquefaction hazard to earthquake risk under sea level rise scenarios.

5. References

Abrahamson N., Silva W., and Kamai R. (2014). Summary of the ask14 ground motion relation for active crustal regions. *Earthquake Spectra*, 30(3): 1025–1055.

Abueladas A-R.A., Niemi T.M., Al-Zoubi A., Tibor G., Kanari M., and Ben-Avraham Z. (2021). Liquefaction susceptibility maps for the Aqaba–Elat region with projections of future hazards with sea-level rise, *Quarterly Journal of Engineering Geology and Hydrogeology*, 54(2).

Befus K.M., Barnard P.L., Hoover D.J., Finzi Hart J.A., and Voss C.I. (2020a). Increasing threat of coastal groundwater hazards from sea-level rise in California. *Nature Climate Change*, 10(10): 946–952.

Befus K.M., Hoover D.J., Barnard P.L., Erikson L.H. (2020b). Projected responses of the coastal water table for California using present-day and future sea-level rise scenarios: U.S. Geological Survey data release. doi: 10.5066/P9H5PBXP.

Bird J.F., Bommer J.J., Crowley H., and Pinho R. (2006). Modelling liquefaction-induced building damage in earthquake loss estimation. *Soil Dynamics and Earthquake Engineering*, 26(1):15-30.

Boore D., Stewart J., Seyhan E., and Atkinson G. (2014). Nga-west2 equations for predicting pga, pgv, and 5% damped psa for shallow crustal earthquakes. *Earthquake Spectra*, 30(3): 1057–1085.

Boulanger R. and Idriss I. (2014). Liquefaction susceptibility criteria for silts and clays. *Journal of Geotechnical and Geoenvironmental Engineering*, 132(11): 1413–1426.

Chiou B. S.-J. and Youngs R. R. (2014). Update of the Chiou and Youngs nga model for the average horizontal component of peak ground motion and response spectra. *Earthquake Spectra*, 30(3): 1117–1153.

Chung J.W., and Rogers J.D. (2013). Influence of assumed groundwater depth on mapping liquefaction potential. *Environmental & Engineering Geoscience*, 19(4): 377-389.

FEMA. (2020). Hazus Earthquake Model Technical Manual. Federal Emergency Management Agency.

Goda K., Atkinson G.M., Hunter J.A., Crow H. and Motazedian D., (2011). Probabilistic liquefaction hazard analysis for four Canadian cities. *Bulletin of the Seismological Society of America*, *101*(1): 190-201.

Grant A.R., Wein A.M., Befus K.M., Hart J.F., Frame M.T., Volentine R., Barnard P., and Knudsen K.L. (2021). Changes in liquefaction severity in the San Francisco Bay area with sea-level rise. In *Geo-Extreme 2021* (pp. 308–317).

Holzer T.L., Toprak S., and Bennett M.J. (2002) Liquefaction potential index and seismic hazard mapping in the San Francisco Bay area, California. *7th National Conference on Earthquake Engineering* (pp. 1699—1706).

Holzer T.L., Noce T.E. and Bennett M.J., (2011). Liquefaction probability curves for surficial geologic deposits. *Environmental & Engineering Geoscience*, *17*(1): 1-21.

Hughes J.D., Langevin C.D., and Banta E.R. (2017). *Documentation for the MODFLOW 6 framework*. 6-A57. [online] USGS Report. doi: 10.3133/tm6A57.

Iwasaki T., Tatsuoka F., Tokida K., and Yasuda S. (1978). A practical method for assessing soil liquefaction potential. *Proceedings of the second International Conference on Microzonation for Safer Construction, Research, and Application* (pp. 885—896).

Kim H-S., Kim M., Baise L.G., and Kim B. (2021). Local and regional evaluation of liquefaction potential index and liquefaction severity number for liquefaction-induced sand boils in Pohang, South Korea. *Soil Dynamics and Earthquake Engineering*, 141:106459.

Koutsourelakis S., Prévost J.H. and Deodatis, G., (2002). Risk assessment of an interacting structure–soil system due to liquefaction. *Earthquake engineering & structural dynamics*, *31*(4):851-879.

Li D.K., Juang C.H. and Andrus R.D. (2006). Liquefaction potential index: A critical assessment using probability concept. *Journal of GeoEngineering*, 1(1): 11–24.

May C. L., Mohan A., Plane E., Ramirez-Lopez D., Mak M., Luchinsky L., Hale T., Hill K. (2022). Shallow Groundwater Response to Sea-Level Rise: Alameda, Marin, San Francisco, and San Mateo Counties. Pathways Climate Institute and San Francisco Estuary Institute.

Moss R., Seed R., Kayen R., Stewart J., Der Kiureghian A., and Cetin K. (2006). Cpt-based probabilistic and deterministic assessment of in situ seismic soil liquefaction potential. *J. Geotech. Goenviron. Eng*., 132(8): 1032–1051.

Murakami S., Yasuhara K., Suzuki N., Wei Ni, and H. Komine. (2005). Vulnerability asessment to liquefaction hazard induced by rising sea-levels due to global warming. In *International Conference on Geotechnical Engineering for Disaster Mitigation & Rehabilitation* (pp. 571–576).

National Academies of Sciences, Engineering, and Medicine. (2021). *State of the Art and Practice in the Assessment of Earthquake-Induced Soil Liquefaction and Its Consequences*. Washington, D.C.: National Academies Press.

Pokhrel R.M., Gilder C.E., Vardanega P.J., De Luca F., De Risi R., Werner M.J. and Sextos A., (2022). Liquefaction potential for the Kathmandu Valley, Nepal: a sensitivity study. *Bulletin of Earthquake Engineering*, *20*(1):25-51.

Shahir H. and Pak A., (2010). Estimating liquefaction-induced settlement of shallow foundations by numerical approach. *Computers and Geotechnics*, *37*(3): 267-279.

Todorovic L. and Silva V., (2022). A liquefaction occurrence model for regional analysis. *Soil Dynamics and Earthquake Engineering*, *161*:107430.

Van Ballegooy S., Malan P., Lacrosse V., Jacka M.E., Cubrinovski M., Bray J.D., O'Rourke T.D., Crawford S.A. and Cowan H. (2014). Assessment of liquefaction-induced land damage for residential Christchurch. *Earthquake spectra*, *30*(1): 31-55.

Wang C. and Chen Q., (2018). A hybrid geotechnical and geological data-based framework for multiscale regional liquefaction hazard mapping. *Géotechnique*, *68*(7): 614-625.

Wang C., Wang D. and Chen Q., (2021). Regional Evaluation of Liquefaction-Induced Lateral Ground Deformation for City-Scale Transportation Resilience Analysis. *Journal of Infrastructure Systems*, *27*(2): 04021008.

Wu M-H., Wang J-P., Wu Y-J. and Chen Z. (2020). Relationship between liquefaction potential index and liquefaction probability. *Journal of GeoEngineering*, 15(3): 135—144.

Zhu J., Baise L.G. and Thompson E.M., (2017). An updated geospatial liquefaction model for global application. *Bulletin of the Seismological Society of America*, *107*(3): 1365—1385.